1	A High-Avidity, Thermostable, and Low-Cost Synthetic Capture for Ultrasensitive
2	Detection and Quantification of Viral Antigens and Aerosols
3	Sean J. Wang <sup>1*</sup> , Rohit Gupta <sup>2</sup> , Ananya Benegal <sup>3</sup> , Rohan Avula <sup>2</sup> , Yin-Yuan Huang <sup>3</sup> , Michael D.
4	Vahey <sup>3</sup> , Rajan K. Chakrabarty <sup>4</sup> , Rohit V. Pappu <sup>3</sup> , Srikanth Singamanenei <sup>2</sup> , Joseph V.
5	Puthussery <sup>4*</sup> , and Matthew R. King <sup>3*</sup>
6 7	<sup>1</sup> Department of Chemistry, Washington University in St. Louis, St. Louis, MO 63130, USA
8	2D CM 1 . 1E 1M 1 G
9	<sup>2</sup> Department of Mechanical Engineering and Materials Science, Institute of Materials Science
10 11	and Engineering, Washington University in St. Louis, St. Louis, MO 63130, USA
12	<sup>3</sup> Department of Biomedical Engineering and Center for Biomolecular Condensates, Washington
13	University in St. Louis, St. Louis, MO 63130, USA
14	
15	<sup>4</sup> Center for Aerosol Science and Engineering, Department of Energy, Environmental and
16	Chemical Engineering, Washington University in St. Louis, St. Louis, MO 63130, USA
17	
18	
19	*To whom correspondence should be addressed:
20	sean.j.wang@wustl.edu (Washington University in St. Louis, 6985 SNOW WAY Dr., St. Louis,
21	MO 63130);
22	matthewking@wustl.edu;
23	joseph.p@wustl.edu;
24	
25	
26	
27	
28	
29	
30	
31	

### Abstract

Lateral flow assays (LFAs) are currently the most popular point-of-care diagnostics, rapidly transforming disease diagnosis from expensive doctor checkups and laboratory-based tests to potential on-the-shelf commodites. Yet, their sensitive element, a monoclonal antibody, is expensive to formulate, and their long-term storage depends on refrigeration technology that cannot be met in resource-limited areas. In this work, LCB1 affibodies (antibody mimetic miniproteins) were conjugated to bovine-serum-albumin (BSA) to afford a high-avidity synthetic capture (LCB1-BSA) capable of detecting the severe acute respiratory syndrome coronavirus 2 (SARS-CoV-2) spike protein and virus like particles (VLPs). Substituting the monoclonal antibody 2B04 for LCB1-BSA (stable up to 60°C) significantly improved the thermal stability, shelf-life, and affordability of plasmon–enhanced lateral flow assays (p-LFAs). Furthermore, this substitution significantly improved the sensitivity of p-LFAs towards the spike protein and VLPs with precise quantitative ability over 2 and 3 orders of magnitude respectively. LCB1-BSA sensors could detect VLPs at 100-fold lower concentrations, and this improvement, combined with their robust nature, enabled us to develop an aerosol sampling technology to detect aerosolized viral particles. Synthetic captures like LCB1-BSA can increase the ultra-sensitivity, availability, sustainability, and long-term accuracy of LFAs while also decreasing their manufacturing costs.

**Keywords:** Lateral flow assay, point-of-care, COVID-19, virus like particles, passive sampling, novel antibody synthesis

Point-of-care (POC) diagnostics are excellent tools for monitoring infectious diseases owing to their ease of use and potential for widespread availability. Most POC diagnostics utilize antibodies as the sensitive element to immobilize a target antigen.<sup>1,2</sup> Dominant among POC modalities are lateral flow assays (LFA), which make up 64.5% of the global point-of-care diagnostic market.<sup>3</sup> LFAs for SARS-CoV-2 now rank alongside pregnancy tests as the two most commonly purchased POC diagnostics, potentially signaling consumer readiness for on-the-shelf diagnostics aimed at other diseases with protein biomarkers like malaria, tuberculosis, and spinal cord injuries.<sup>4–7</sup> However, in developing countries and rural areas, poor external quality control and procurement challenges pose a major operational barrier for these diagnostics. Antibodies are known to be unstable as diagnostic tools because they are prone to aggregation and have low thermal stability.<sup>8</sup> Furthermore, monoclonal antibody production requires significant upfront capital investment and involves high production costs, primarily to mitigate against unwanted post-translational modifications and intrinsic pH sensitivity.<sup>9</sup> Compunding these expenses, antibodies need to be refrigerated during transportation and long-term storage.<sup>10</sup>

Previously, many groups have reported the use of aptamers (nucleic acid affinity probes) and miniproteins (synthetic protein affinity probes) as captures for LFAs. <sup>11–13</sup> Compared to antibodies, both captures are thermally stable, economical, and comparably easier to synthesize in-vitro using systematic evolution of ligands by exponential enrichment (SELEX) for aptamers and phage display for miniproteins. <sup>14,15</sup> However, the recent advancements in protein engineering have made it possible to design miniproteins completely de-novo, albeit with certain limitations in analyte size and complexity. <sup>16,17</sup> Thus, we wanted to explore the potential of de-novo protein engineering for rapid deployment of thermally stable LFAs by developing a robust sythetic capture based on affibody (<100 amino-acid-long, highly thermostable 3 or 4-fold alpha helix bundles) technology with the purpose of detecting the SARS-CoV-2 spike protein.

In this paper, we utilized the previously engineered and validated LCB1 affibody, which harbors both high thermal stability (T<sub>m</sub> > 95°C) and high spike protein binding affinity (K<sub>d</sub> < 1nM).<sup>18</sup> Our design comprises multiple LCB1 affibodies conjugated to Bovine Serum Alblumin (BSA) to yield a high-avidity, thermostable detector termed LCB1-BSA. Recently, we introduced a plasmonic-fluor-based LFA (p-LFA) and a plasmonic-fluor-based immunosorbent assay (p-FLISA) that

utilized the ultrabright plasmonic-fluor (PF) nanolabel to enhance the sensitivity of conventional gold nanoparticle and molecular fluorophore based LFAs 1000-fold; p-LFA can also be imaged by our recently introduced inexpensive (<\$1000) fluorescent scanner, which is designed specifically for point-of-care uses and has comparable sensitivity to laboratory–grade instruments.<sup>19</sup> Building off our previous work, we combined LCB1-BSA's robustness and p-LFA's ultrasensitivity to create a truly point-of-care diagnostic with unmatched sensitivity, affordability, and outreach.

LCB1-BSA improved the shelf-life and thermal stability of p-LFAs harboring an industry-standard monoclonal antibody with no change to existing protocol. The high-avidity of LCB1-BSA also improved the dynamic range of SARS-CoV-2 spike protein and virus like particle (VLP) quantification. VLPs are structurally mimicking pseudoviruses without genetic material.<sup>20</sup> Being noninfectious, they allowed us to explore a novel possibility with our robust and ultrasensitive LCB1-BSA sensor: a proof-of-concept passive sampling technique for VLP aerosol detection with the goal of fabricating a "point-of-need" sensor for indoor surveillance of SARS-CoV-2 in high-risk-areas like ICU rooms, airplanes, and crowded spaces.

### **Materials and Methods**

### **Total Synthesis of LCB1-BSA**

LCB1 affibodies were modified to include an octa-histidine tag and C-terminal cysteine residue and expressed and harvested from bacteria. The terminal cysteine allowed for the conjugation of BSA and LCB1 via a sulfo-amide crosslinker (SI **Figure S1B**). We used size exclusion chromatography to purify conjugated BSA-LCB1 proteins from free LCB1 (**SI Figure S1C**). SDS-PAGE analysis of purified LCB1-BSA revealed several uniformly spaced bands with ~15 kDa intervals from 90 to 170 kDa (**SI Figure S1D**). These bands correspond to multiple LCB1 proteins conjugated to a single BSA protein (LCB1 apparent MW = 15 kDa, BSA MW = 66 kDa) (**Figure S1D**). By comparison, a monoclonal IgG antibody (mAb) contains 2 antigen binding sites while LCB1-BSA can contain upwards of 6 antigen binding sites. The specificities of our synthesis are available in the supplementary information.

# Spike protein and VLP plasmon-enhanced fluorescence immunoassay (p-FLISA) and

- plasmonic-enhanced lateral flow assay (p-LFA)
- A detailed protocol to prepare and measure p-FLISA and p-LFA is available in the supplementary
- information. Many of these steps are referred to in our following experiments. The protocol to
- 128 synthesize and quantify VLPs is also in the supplementary information. The preliminary
- interference testing procedure is also detailed in the supplementary information. Schematics
- illustrating the processing of well-based p-FLISAs and paper-based p-LFAs are in Figures 1A,
- 2A respectively. To assess the performance of each assay, we calculated their Limit-of-Detection
- (LoD) and Resolution of molecular concentration (RMC). LoD represents the minimum sensitivity
- of an assay while RMC is a metric that determines whether two different analyte concentrations
- can be distinguished with statistical significance.<sup>21</sup> Specifically, the calculated RMC µ parameters
- are the changes in concentrations that can be distinguished with 99% certainty and assay is
- considered quantitative if it can resolve <100% changes ( $\mu<2$ ) in analyte concentrations. With
- 137 RMC, we can quantify the dynamic sensitivity of an assay across a range of analyte concentrations
- 138 (Figure 3). A description of on how RMC is computed is available in the supplementary
- information.

140141

124

# Thermal stability comparison of LCB1-BSA and 2B04 antibody on p-LFA

- Half-stick p-LFAs (Figure 2A) containing LCB1-BSA or 2B04 were prepared and placed in
- plastic petri-dishes wrapped with parafilm. They were then incubated at 23°C, 40°C, and 60°C
- 144 respectively. To further understand the thermal stability of LCB1-BSA p-LFAs,
- pre-sliced nitrocellulose strips and an aliquot of 1mg/mL LCB1-BSA solution were also incubated
- at 60°C. At certain time intervals (Day 1, 4, 7, 14, 21; Figure 4), the prepared half-stick p-LFAs
- were extracted and exposed to 100μL of analyte standard (1μg/mL VLP or 400ng/mL spike
- protein) and 1mg/mL 2E06 detection antibody. For the variable component p-LFAs, the incubated
- 149 nitrocellulose strips were exposed to fresh LCB1-BSA and blocked with fresh BSA while the
- heated LCB1-BSA was pipetted onto fresh nitrocellulose strips and blocked with fresh BSA.

151

152

### Aerosol chamber construction and sampling of SARS-CoV-2 VLP Aerosols

- VLPs were aerosolized via a cough-simulating nebulizer and captured on 4-well p-FLISA plates
- and p-LFA sample pads protected within 3D printed cassettes. Both collectors were placed either

7 inches in front of the nebulizer (representing detection from a person coughing) or at the back of the vent (representing detection of diluted aerosols in a closed room). The aerosol chamber is 60cm x 42cm x 34cm in size and a schematic is provided in **Figure 5A**. Further details regarding these procedures and the post-aerosolization sample processing are provided in the supplementary information.

### Results and discussion

# **Facile Synthesis of LCB1-BSA**

The process of producing LCB1-BSA is significantly easier and cheaper compared to mAb production. Currently, antibodies are harvested from hamster ovary cell lines, which require specific culture conditions and a 5-14 day incubation period to reach optimal cell density.<sup>22</sup> This process is both labor and resource intensive, requiring for example, frequent cell passaging and mitigation against contamination by microorganisms.<sup>22,23</sup> The space time yields are also variable and dependent on antibody complexity and formulation, ranging from 0.050–5g/L\*day.<sup>22,24</sup> In Japan, the operating cost of mAb cultivation averages \$80,000/kg, mostly due to expensive culture media that is formulated to stabilize cell culture pH and be devoid of metabolites that could promote deleterious post-translational modifications.<sup>23</sup> On the other hand, bacteria cultures are robust and can reach an optimal cell density in 1-2 days. Thus, small recombinant proteins like LCB1 can be easily generated for under \$45/kg (based on recombinant soy peptone production cost) with easily achievable >1g/L\*day space time yields.<sup>25–27</sup> For the total synthesis of LCB1-BSA, we estimate that it would be under \$100/kg. Thus, affibody-based POC tests, such as the LCB1-BSA p-LFA rapid SARS-CoV-2 test developed here, have the potential of widespread availability as they can be produced or purchased readily.

# LCB1-BSA has superior detection capabilities compared to 2B04 monoclonal antibody

To validate the detection capabilities of LCB1-BSA, we compared its sensitivity with 2B04, a traditional monoclonal antibody on the p-FLISA and p-LFA platforms. p-FLISA is a 4-hour well-based assay, which is similar to the gold-standard enzyme-linked immunosorbent assay (ELISA), while p-LFA is a 15-minute paper-based assay (**Figures 1A, 2A**). The importance of validating LCB1-BSA on both assays is to ensure that the capture can serve as a substitute for the two most used antibody-based assays. The use of ultrabright plasmonic-fluor (PF) as our nanolabel is also

essential for comparing the quantitative sensitivities of LCB1-BSA and 2B04 on the p-LFA platform since traditional nanolabels like gold nanoparticles or molecular fluorophores are not inherently sensitive enough to allow for detailed quantitative detection.<sup>19</sup>

p-FLISA and p-LFA SARS-CoV-2 spike antigen assays using LCB1-BSA had similar LoDs when compared to 2B04 based assays (**Figures 1B, 2B, 2C**). However, LCB1-BSA was 100 times more sensitive (100x lower LoD) towards the detection of VLPs than 2B04 (**Figure 1B**). LCB1-BSA based p-LFAs also maintained a similar limit of detection with its p-FLISA counterpart for the detection of VLPs, demonstrating that the bulky and large VLPs do not lead to noticeable non-specific binding or membrane pore blockage under 10ng/mL (**SI Figure S2C**). Interference testing of LCB1-BSA against endemic viruses influenza and respiratory syncytial virus was also performed (**SI Figure S3**).

To assess the ability of LCB1-BSA to quantify spike protein and VLP concentrations, we calculated their RMCs. Using RMC, we discovered that none of the 2B04 based assays were able to distinguish less than 2-fold, or 100%, changes (μ=2) in spike protein or VLP concentration (SI Table S1). However, when measuring spike protein concentration, LCB1-BSA based p-FLISA and p-LFAs were able to resolve <100% changes in spike protein concentration across 2 orders of magnitude and <100% changes in VLP concentration across 3 orders of magnitude (Figures 3C, 3B). The significant enhancement in sensitivity is likely due to 2 major differences between the 2B04 mAb and LCB1-BSA captures. Firstly, the spike protein has 3 receptor binding domains (RBD), and it has been well-established that multivalent target binding decreases the ligand-receptor dissociation constant and can promote positive cooperativity.<sup>28</sup>

LCB1-BSA based assays, however, exhibit non-cooperative binding (Hill coefficient (n) ~0.9-1) and implies that the LCB1 affibodies are not in close proximity since it has been previously reported that non-cooperative binding of multivalent systems can occur if the binding sites are not in close proximity (SI Table S1).<sup>29</sup> Thus, it appears that LCB1-BSA multivalency stabilizes the spike-affibody and VLP-affibody complex through multisite binding.

On the other hand, the Hill coefficient for 2B04 based assays was n~0.7 for both the detection of spike protein and VLPs, indicating negative cooperativity (SI Table S1). Since 2B04 can only bind the spike RBDs with a maximum multivalency of 2, it is unable to take full advantage of its multivalency and cannot stabilize the spike-antibody complex as well as LCB1-BSA. Both LCB1 and 2B04 also bind the spike RBD strongly (<1nM and ~1nM respectively), so the lack of ultrasensitivity in 2B04 based assays cannot be attributed to a difference in binding affinity, but rather an opportunity for high-avidity binding. A detailed description of our RMC calculations, Hill coefficient calculations, and choices for curve fitting is available in the supplementary information.

Secondly, proteins will bind to the ELISA polystyrene well or LFA nitrocellulose paper via weak electrostatic and hydrophobic interactions, leading to protein binding in random orientations. This decreases the density of accessible binding sites of mAbs like 2B04 from its maximal 2 sites to between 0-2 sites (Figure 3C). And despite more sophisticated measurements confirming LCB1's high-affinity, using LCB1 by itself as a capture for p-LFA did not yield a quantifiable signal, likely because its small size caused it to be bound to the nitrocellulose membrane in an inaccessible conformation (Fig. 3C). Specifically, LCB1 contains a 2 alpha-helix binding domain and 1 alphahelix scaffolding domain, so the face-down conformation may be preferable because it maximizes the intermolecular interactions with the membrane. Conversely, in LCB1-BSA, 2-6 binding domains (i.e., affibodies) were attached to a bulky BSA scaffold via a flexible peptide linker. This design likely ensures that there will always be 1-6 binding sites available, creating high-density regions that optimize multivalent binding and analyte distribution (Figure 3C). While other techniques have utilized chemical functionalization of the LFA membrane and capture to induce correct orientation of aptamer or antibody captures, LCB1-BSA can be seamlessly integrated without any procedural modifications because the intermolecular forces governing its immobilization is the same for antibodies.<sup>31–33</sup>

Our results are also substantiated by previous studies that have reported minor sensitivity increases (quantified by LoD improvement) from increased capture density, avidity, or improved antibody orientation.<sup>31,32,34</sup> By analysis with RMC and Hill-coefficients, we were able to demonstrate a significant improvement in LFA quantitation due to LCB1-BSA multivalency that has yet to be reported.

248 LCB1-BSA based p-LFAs have enhanced shelf life and thermal stability compared to 2B04

249 monoclonal antibody-based p-LFAs

Next, we sought to assess the sensitivity and thermal stability of LCB1-BSA based p-LFAs. Half-

strip p-LFAs utilizing LCB1-BSA or 2B04 were fabricated and incubated at room temperature

252 (RT), 40°C, and 60°C. Over a period of 14 days, the p-LFAs were exposed to a spike protein

standard and their performance was validated in the form of retained biorecognition, which was

quantified by dividing the Signal to Noise Ratio (SNR) of treated p-LFAs by the SNR of a fresh

255 Day 0 p-LFA.

256

259

260

261

262

263

253

254

257 Although both LCB1-BSA based and 2B04 based p-LFAs performed similarly at RT (~90%

biorecognition after 14 days), LCB1-BSA based p-LFAs retained ~85% of their biorecognition

capability after 14 days at 40°C, compared to the ~65% afforded by 2B04 based p-LFAs (Figures

4A, 4B). This suggests that LCB1-BSA would have the longer shelf-life due to its higher thermal

stability (implying higher activation energy and longer denaturation time according to a previously

reported modified Arrhenius expression).<sup>35</sup> Similarly, for the detection of VLPs, the LCB1-BSA

based p-LFAs demonstrated similar trends in retained biorecognition (~90% after 14 days)

(Figures 4C). Significantly, this similarity affirms that multivalent binding is still available.

264265

267

268

269

270

271

272

273

274

275

276

At 60°C, both the detection capabilities of 2B04 and LCB1-BSA based p-LFAs experienced rapid

degradation (Figures 4A, 4B). This may be due to nitrocellulose test membrane degradation at

60°C rather than LCB1-BSA denaturation (SI Figure S4). And while BSA denatures at 63°C, we

show that drop casting LCB1-BSA, incubated over the same period at 60°C, onto fresh LFA test

membrane had no impact on the performance of p-LFA, suggesting that BSA only acts as a

scaffolding protein (SI Figure S4). Yet, we observe that the effect of test membrane degradation

on the retained biorecognition decreases linearly and converges with the 60°C incubated p-LFA

after 7 days. The significant initial drop (day 1) in retained biorecognition of p-LFA implies a

partial degradation of LCB1-BSA. We hypothesize that LCB1-BSA is fusing to the membrane on

carbon 6 of nitrocellulose, since its -ONO<sub>2</sub> functional group can undergo thermolysis into a free

radical or act an excellent leaving group. Nonetheless, LCB1-BSA ensures the long-term usability

and stability of p-LFA.

279 Passive virus aerosol sampling using LCB1-BSA 280 Finally, we developed a technique using LCB1-BSA to sample and detect SARS-CoV-2 VLPs as 281 a proof-of-concept for identifying airborne viral pathogens. An aerosol chamber was constructed 282 to simulate an enclosed space with a strong vent that could represent an airplane, an ICU room, 283 or a crowded indoor space (Figure 5A). Aerosols with sizes mimicking coughing were 284 produced, captured, and detected on p-LFA sample pads and p-FLISA wells (SI Figure S5). 285 286 Both platforms were able to detect VLP aerosols (Mean fluorescence signal or SNR > LoD of 287 assay) produced directly in front of the sneeze generator under all conditions (Figures 5B, 5C). 288 However, it should be noted that the proper vertical alignment of the p-LFA during the 289 experiment posed a challenge, which may have contributed to the limited aerosol collection at 290 0.6 ml/min (Figure 5C). Nonetheless, these results demonstrate a proof-of-concept passive 291 sampling technique that could be used to inform the user if they have been directly exposed to a 292 person with SARS-CoV-2 or an area contaminated with the virus. To simulate the detection of 293 circulating VLPs in an indoor building, p-FLISAs and sample collecting pads were placed 294 directly in front of the chamber vent (Figure 5A). p-FLISA successfully detected VLPs at 0.6 295 ml/min and 0.9 ml/min while p-LFA could only detect them at 0.9 ml/min (Figures 5B, 5C). 296 This outcome was unexpected since we anticipated that the large surface area and absorptive 297 nature of the sample collecting pad would excel in capturing the VLP aerosols. However, the 298 requirement for the LFA test membrane width to match the sample pad width led to a more 299 spread-out and less dense test spot containing LCB1-BSA than a traditional LFA (with a 3mm 300 width), resulting in reduced sensitivity. For future experiments, a trapezoidal shaped sample pad 301 with a 3 mm and 5.5 mm base would offer a larger surface area to capture VLPs and allow us to 302 increase the test spot signal density. 303 It is important to emphasize that even though the ventilation rate and VLP quantities may exceed 304 typical indoor conditions, future applications can consider the use of aerosol-concentrating devices, such as high-flow cyclone air samplers, to funnel viruses onto a concentrated point for 305 highly efficient detection.<sup>36</sup> Nonetheless, these results underscore the effectiveness of the wells 306 307 and sample collecting pads for the collection of SARS-CoV-2 virions and other pathogens with 308 high shedding rates in indoor environments.

### **Conclusion and Outlooks**

LCB1-BSA can significantly prolong the shelf-life of any SARS-CoV-2 antibody-based diagnostic and decrease their manufacturing costs. Furthermore, many problems in antibody manufacturing like aggregation and thermal instability can be avoided by using affibody-based captures like LCB1-BSA. However, our reported sensitivity improvements may only be applicable to assays with inherent ultrasensitivity like p-LFA and surface-enhanced Raman scattering (SERS) based LFAs. Further experiments are needed to explore LCB1-BSA's ability to improve the sensitivity of current on-the-shelf colorimetric LFAs. Nonetheless, LCB1-BSA demonstrates the potential of synthetic, multivalent captures as being superior to monoclonal antibodies for POC diagnostics that can be manufactured significantly cheaper and faster. Aside from multivalent analytes, the optimal analyte distribution provided by LCB1-BSA may also improve the sensitivity of assays that target smaller, single epitope analytes like the SARS-CoV-2 nucleocapsid protein, but only when compared to antibodies with similar binding affinity to the affibody.

Further experiments should assess the sensitivity of LCB1-BSA against SARS-CoV-2 variants and explore an alternative synthesis of an in tandem conjugated LCB1 (similar to IgM polyclonal antibodies). This process could overcome the extra BSA conjugation step and be even simpler and cheaper. Moreover, increased thermal stability should allow affibody-based assays to be easily transported to any location. With such potential for wide availability and affordability, pre-emptive screening would be more efficient, allowing individuals to quarantine faster and healthcare workers to contain and track viral spread. Furthermore, our method of affibody conjugation can also be applied to develop synthetic captures with different affibodies for multiplex detection capabilities.

Outside of POC diagnostics, the combination of ultra-sensitivity and high speed (15 minutes to perform) that affibody-conjugated BSA based p-LFA offers could be useful as a research tool to quantify a wide range of viruses, complementing or potentially replacing traditional viral quantification assays like western blots (hours) and plaque assays (days). Furthermore, the sensitivity of the western blot is highly dependent on antibody quality and fluorescence imaging device sensitivity. The first issue can be resolved by rapidly improving computational affibody design, whereas the second issue has already been resolved with our inexpensive fluorescent

scanner for p-LFA. <sup>16,19</sup> Lastly, the LCB1 affibody serves as an example of the burgeoning field of generative biology, designed *de novo* for the specific purpose of binding Spike protein. What used to take years for the generation of bespoke affibodies like LCB1, can now theoretically be done in days. And although many state-of-the-art generative models like RFDiffusion have low success rates for high affinity binders and still rely on experimental validation, they will continue to improve as experimental data, NMR structural refinement, and protein molecular dynamics using highly accurate protein forcefields are used to enhance the accuracy of these neural networks and their binding affinity predictions. <sup>17</sup> Thus, our work serves as a proof-of-concept for how one can leverage advances in protein design to create reliable and low-cost POC diagnostics.

Finally, our novel proof-of-concept implementation of LCB1-BSA as a sensor for a passive sampling may be more economical, practical, and faster compared to traditional reverse transcriptase polymerase chain reaction (RT-PCR) viral sampling approaches that require separate aerosol capturing devices and detect RNA, which is unstable when exposed to air. <sup>38,39</sup> By incorporating sample collection pads into face masks, individuals could be alerted to potential viral exposure after analysis of the collected samples. When these pads are placed in air vents, they can monitor the presence of viruses within indoor environments, as depicted in **Figure 6**. While this method would not offer instantaneous results, it is invaluable for monitoring high-risk environments such as airplane cabins, intensive care units, and crowded venues. Future experiments should focus on comparing the collection efficiency of our technique versus conventional techniques and improving the repeatability of our technique to allow for the exploration of quantitative aerosol sampling using LCB1-BSA.

# **Supporting Information**

- The Supporting Information Available: The following files are available free of charge at
- 365 "Supplementary information"
  - Descriptions of synthetic, experimental, measurement details, RMC and curve-fitting calculations.
  - LCB1-BSA synthesis, p-LFA fluorescent readouts, interference testing, thermal stability, and VLP aerosol distribution supplementary figures

### 371 Figures

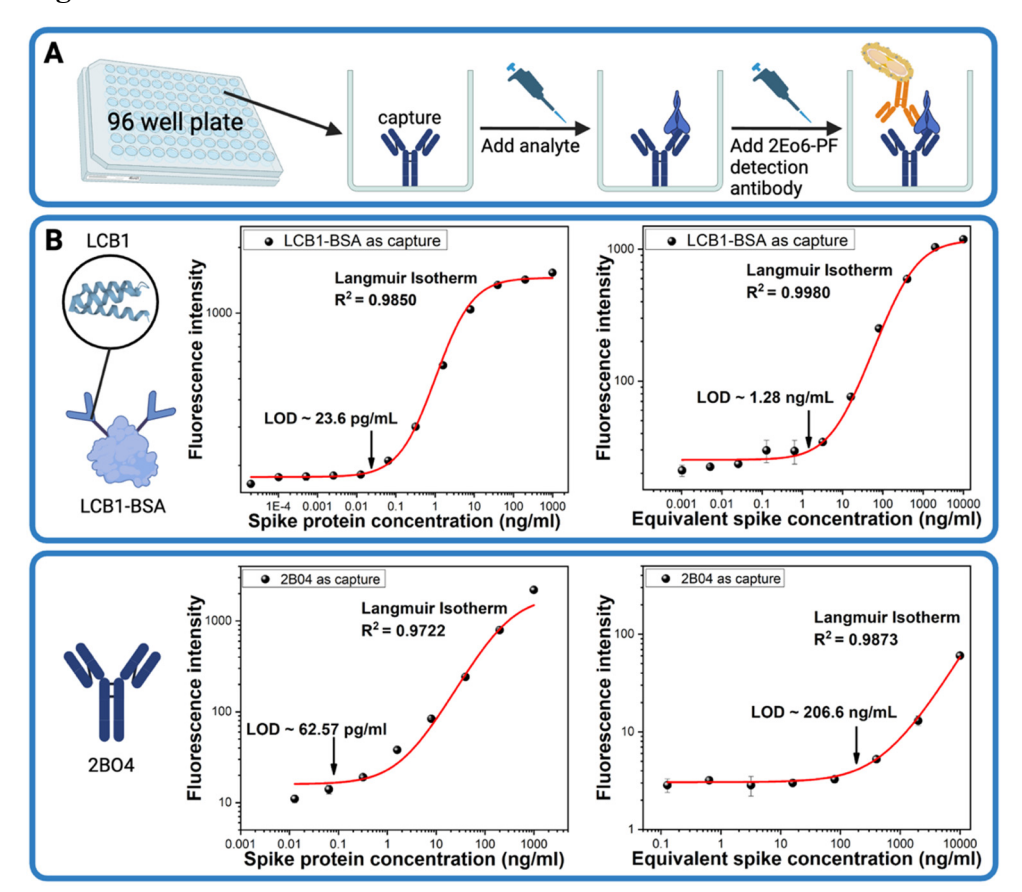
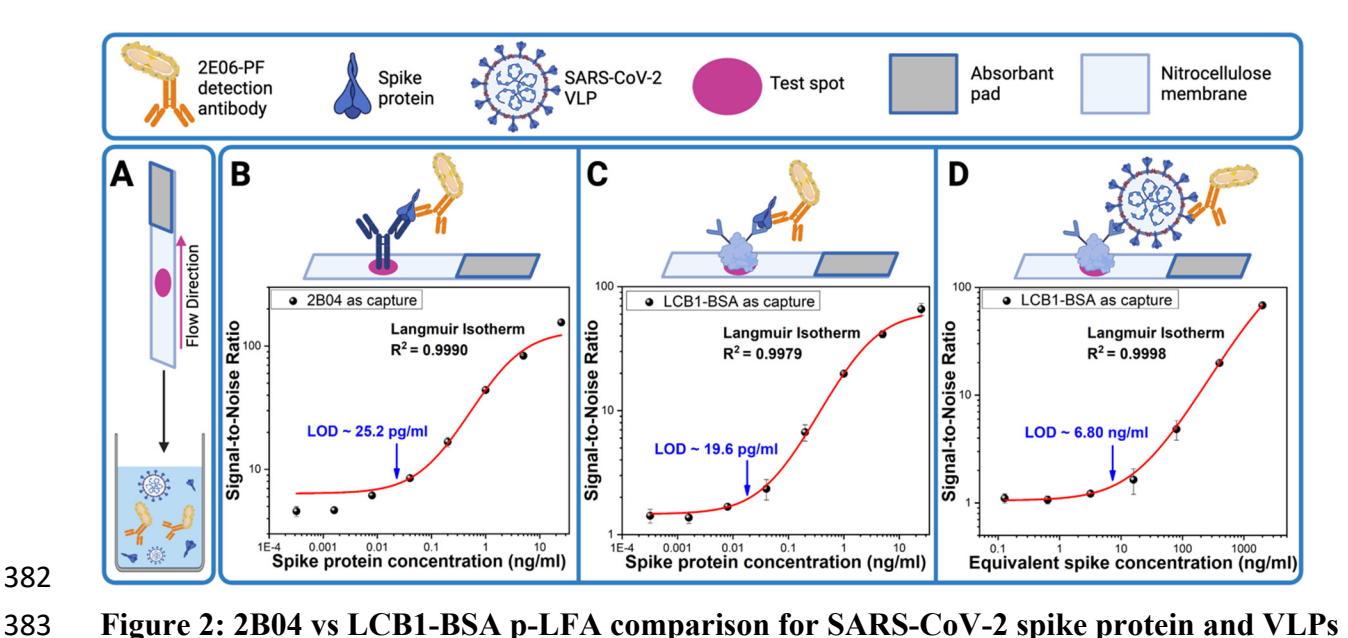


Figure 1: 2B04 vs LCB1-BSA p-FLISA comparison for SARS-CoV-2 spike protein and VLPs (A) Schematic illustration of p-FLISA procedure which adds analyte and detection antibodies stepwise into small wells coated with capture antibody. (B) p-FLISA detection of spike protein and SARS-CoV-2 VLP serial dilutions (n=2) using LCB1-BSA (top panel) or 2B04 as (bottom panel). For the standard curve of VLPs, we reported the concentration in equivalent spike concentration, which represents the concentration of spike protein in the VLP standard. The Limit of Detection (LoD) is represented with an arrow and is defined as the mean signal from the final dilution (designated as the blank) or the first point of the Langmuir curve  $+3\sigma$  of the blank.



**Figure 2: 2B04 vs LCB1-BSA p-LFA comparison for SARS-CoV-2 spike protein and VLPs** (**A**) Schematic illustration of p-LFA half-strips, which comprise of a test spot and can detect either spike protein or spike protein bound on SARS-CoV-2 VLPs. (**B**) Standard curves of p-LFA spike protein detection with 2B04 (n=2). The Limit of Detection (LoD) is represented with an arrow and defined as the mean signal from the final dilution (designated as the blank) + 3σ of the blank. (**C**) Standard curves of p-LFA spike protein detection with LCB1-BSA (n=2). (**D**) Standard curves of p-LFA VLP detection in equivalent spike concentration with LCB1-BSA (n=2). We omitted the last datapoint (10μg/mL) from the curve for better curve fitting due to the extremely high background signal, which we hypothesize to be from membrane pore blockage caused by high

concentrations of VLPs.

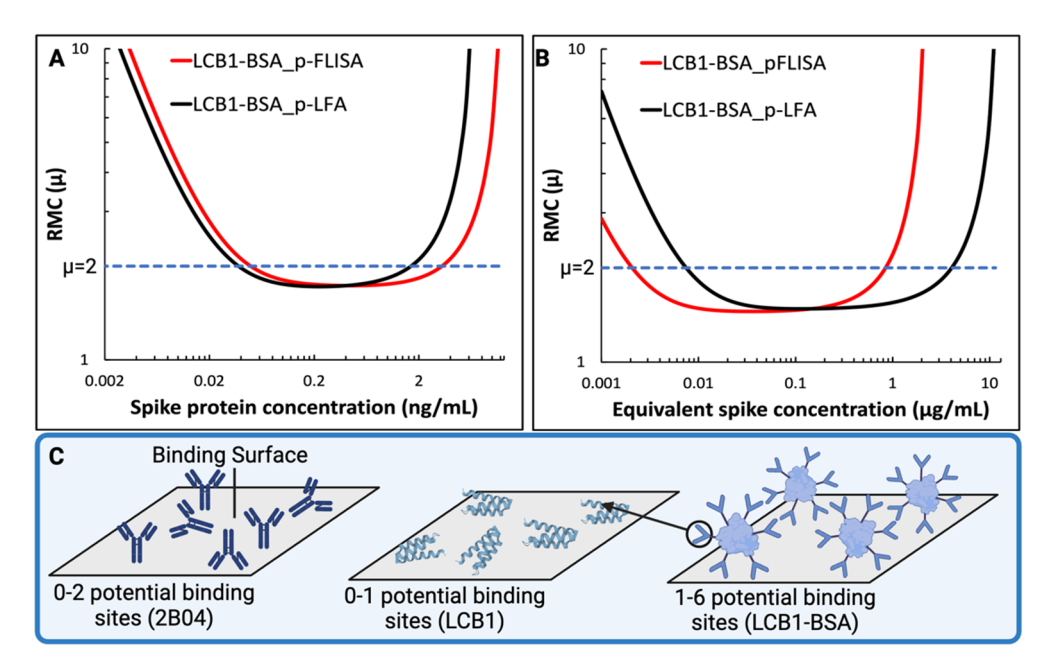


Figure 3: Quantitative ultrasensitivity of LCB1-BSA based p-FLISA and p-LFA

(A) RMC curves for spike protein assays. The dashed blue line represents the  $\mu$ =2 cutoff. For LCB1-BSA based p-FLISA,  $\mu$ <2 over a concentration range of 0.050-3.31 ng/mL with a  $\mu_{min}$ =1.73 at 0.43 ng/mL. For LCB1-BSA based p-LFA,  $\mu$ <2 over a concentration range of 0.038-1.68 ng/mL with a  $\mu_{min}$ =1.72 at 0.22 ng/mL. (B) RMC curves for VLP assays. For LCB1-BSA based p-FLISA,  $\mu$ <2 over a concentration range of 2.1-846 ng/mL with a  $\mu_{min}$ =1.45 at 33 ng/mL. For LCB1-BSA based p-LFA,  $\mu$ <2 over a concentration range of 7.5-4070 ng/mL with a  $\mu_{min}$ =1.48 at 11 ng/mL. (C) Diagram showing how the different orientations of immobilized capture can affect the number of exposed binding sites.

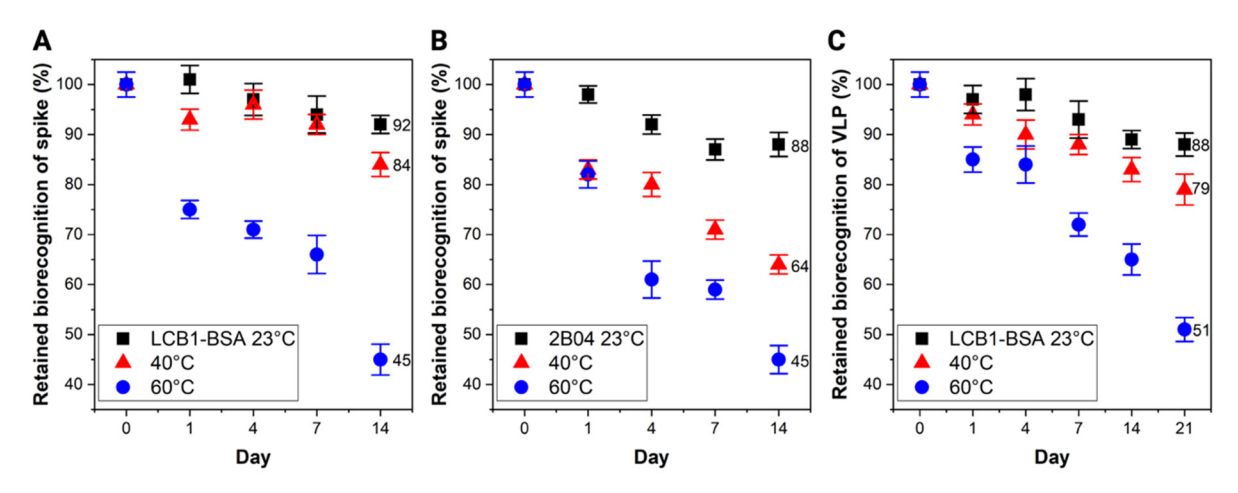


Figure 4: 2B04 vs LCB1-BSA thermal stability comparison

**(A)** Retained biorecognition of half-Stick p-LFAs at RT, 40°C, and 60°C with LCB1-BSA as the capture for spike protein over 14 days (n=2). **(B)** Retained biorecognition of Half-Stick p-LFAs at RT, 40°C, and 60°C with 2B04 as the capture for spike protein over 14 days (n=2). **(C)** Retained biorecognition of Half-Stick p-LFAs at RT, 40°C, and 60°C with LCB1-BSA as the capture for VLPs over 21 days (n=2). For day 0, 6 samples were used to establish the baseline SNR.

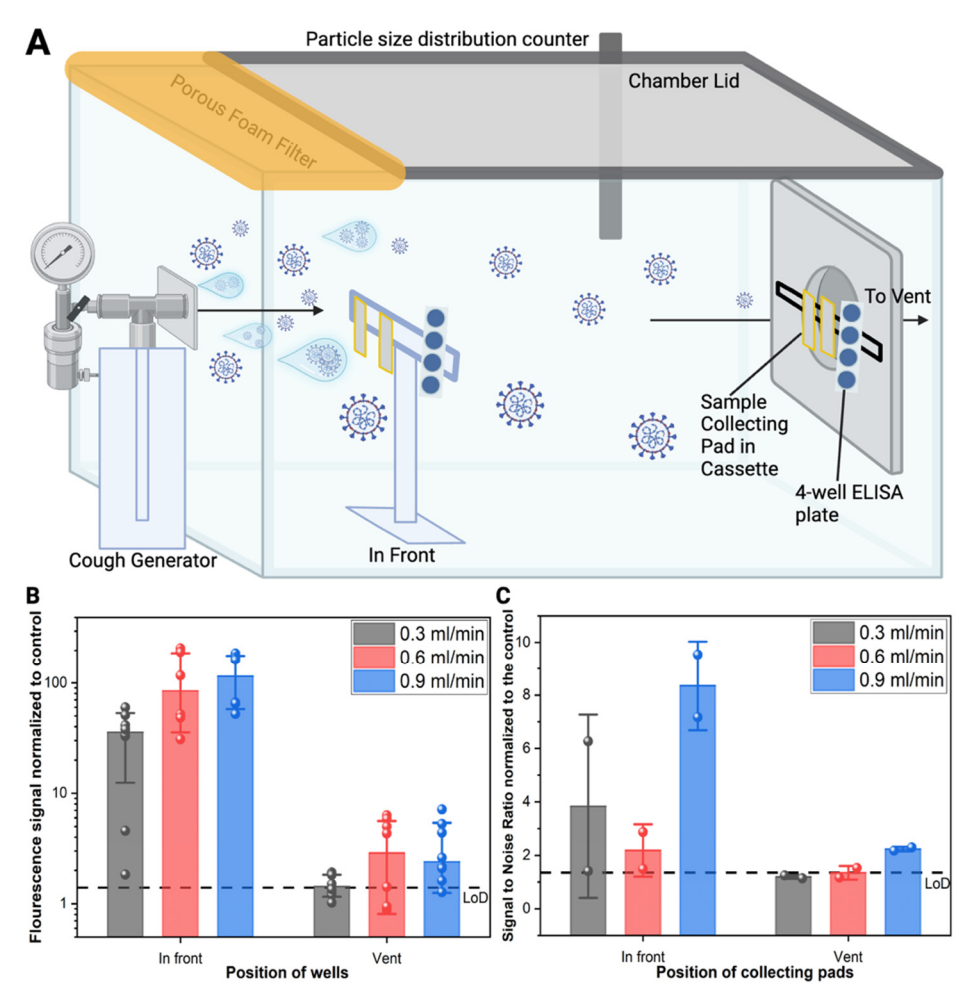


Figure 5: Performance testing of LCB1-BSA to sample VLP aerosols

(A) Aerosol test chamber schematic. The aerosol test chamber with the BLAM nebulizer and test strips was placed in the fume hood. The 4 wells and 2 sample collecting pads were placed "In front" of the BLAM nozzle (7" from the nozzle), and over the "Vent" outlet. The dashed black line shows the LoD of the measurements calculated as the mean blank signal  $+ 3\sigma$ . (B) The fluorescence signal after normalizing with the blank for the cough aerosol generation conditions (0.3, 0.6, and 0.9 mL/min of a 900ng/mL VLP stock solution, corresponding to 270, 540, and 810 ng/mL aerosolized solution) for the p-FLISA well collecting platforms (n = 4 wells per test condition, and each experiment was repeated twice at each test condition). (C) The SNR after normalizing with the blank for the different aerosol generation conditions for the p-LFA sample pad collecting platforms (n = 2 p-LFA strips per test condition, and samples were collected once for each test condition).

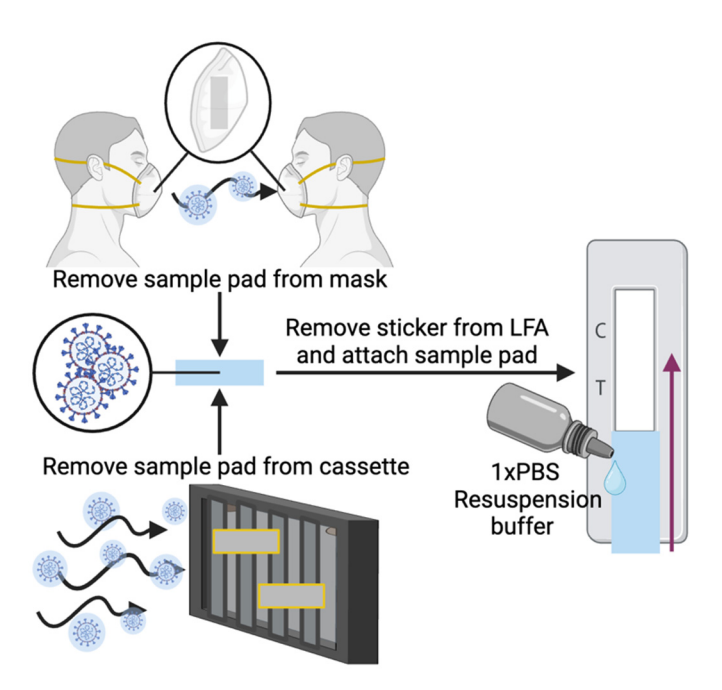


Figure 6: Proposed applications for passive sampling of SARS-CoV-2 using the sample collecting pad and p-LFA platform.

The sample collecting pad could be inserted into face masks, removed, and tested later to inform the user if they have been exposed to an infected individual. Furthermore, the sample collecting pad could be placed over strong, indoor vents in ICU rooms or airplanes for indoor environmental passive sampling.

De-novo affinity Thermally stable (60°C) Inexpensive High-avidity

LCB1-BSA Synthetic Antibody

LCB1
Spike receptor binding domain

TOC Graphic: Schematic and key properties of LCB1-BSA

### 443 Acknowledgements:

- We acknowledge the support from National Science Foundation (S.S.: CBET-2224610, N and
- 445 CBET-2316285); (M.D.V: 2029105); NIH / NIGMS fellowship funding (M.R.K.: F); WashU-
- 446 IITB Joint Master's program (J.V.P.), a gift from The Flu Lab (J.V.P. and R.K.C.). All figures
- were created and organized in BioRender. All graphs were plotted in OriginPro.

448

### 449 Author Contributions:

- 450 S.S., S.W., R.G., M.R.K. conceptualized the project. M.R.K., R.G., S.W. synthesized LCB1-
- 451 BSA. A.B., M.D.V. provided the VLPs. S.W., R.G. performed the p-LFA, p-FLISA, and
- 452 thermostability experiments. S.W., J.V.P. performed the aerosolization experiments. R.A., Y.H.,
- S.W. performed the interference experiments. S.S. reviewed the data and provided feedback.
- 454 S.W. wrote the original draft. All authors reviewed and edited the final draft.

455

456

#### **Declaration of interest:**

- S.S. is an inventor on a pending patent related to plasmonic-fluor technology and the technology
- has been licensed by the Office of Technology Management at Washington University in St.
- Louis to Auragent Bioscience LLC. S.S. is a co-founder/shareholder of Auragent Bioscience
- 460 LLC. S.S. along with Washington University may have financial gain through Auragent
- 461 Bioscience, LLC through this licensing agreement. These potential conflicts of interest have been
- disclosed and are being managed by Washington University in St. Louis.

463

464

### References:

- (1) Heidt, B.; Siqueira, W. F.; Eersels, K.; Diliën, H.; van Grinsven, B.; Fujiwara, R. T.; Cleij, T.
   J. Point of Care Diagnostics in Resource-Limited Settings: A Review of the Present and
   Future of PoC in Its Most Needed Environment. *Biosensors* 2020, 10 (10), 133.
- https://doi.org/10.3390/bios10100133.
- 469 (2) Qin, J.; Wang, W.; Gao, L.; Yao, S. Q. Emerging Biosensing and Transducing Techniques 470 for Potential Applications in Point-of-Care Diagnostics. *Chem. Sci.* **2022**, *13* (10), 2857– 471 2876. https://doi.org/10.1039/D1SC06269G.
- 472 (3) Lateral Flow Assays Market Size And Share [2023 Report].
- https://www.grandviewresearch.com/industry-analysis/lateral-flow-assay-market (accessed 2023-08-15).
- 475 (4) Koczula, K. M.; Gallotta, A. Lateral Flow Assays. *Essays in Biochemistry* **2016**, *60* (1), 111– 120. https://doi.org/10.1042/EBC20150012.

- (5) Kim, J.; Cao, X. E.; Finkelstein, J. L.; Cárdenas, W. B.; Erickson, D.; Mehta, S. A Two-Colour Multiplexed Lateral Flow Immunoassay System to Differentially Detect Human Malaria Species on a Single Test Line. *Malaria Journal* 2019, *18* (1), 313. https://doi.org/10.1186/s12936-019-2957-x.
- (6) Nathavitharana, R. R.; Lederer, P.; Chaplin, M.; Bjerrum, S.; Steingart, K. R.; Shah, M.
   Impact of Diagnostic Strategies for Tuberculosis Using Lateral Flow Urine
   Lipoarabinomannan Assay in People Living with HIV. Cochrane Database of Systematic
   Reviews 2021, No. 8. https://doi.org/10.1002/14651858.CD014641.
- 485 (7) Gonuguntla, S.; Herz, J. Unraveling the Lymphatic System in the Spinal Cord Meninges: A
  486 Critical Element in Protecting the Central Nervous System. *Cell. Mol. Life Sci.* **2023**, *80*487 (12), 366. https://doi.org/10.1007/s00018-023-05013-1.
- 488 (8) Ma, H.; Ó'Fágáin, C.; O'Kennedy, R. Antibody Stability: A Key to Performance Analysis,
   489 Influences and Improvement. *Biochimie* 2020, 177, 213–225.
   490 https://doi.org/10.1016/j.biochi.2020.08.019.
- (9) Yan, Y.; Liu, A. P.; Wang, S.; Daly, T. J.; Li, N. Ultrasensitive Characterization of Charge
   Heterogeneity of Therapeutic Monoclonal Antibodies Using Strong Cation Exchange
   Chromatography Coupled to Native Mass Spectrometry. *Anal. Chem.* 2018, 90 (21),
   13013–13020. https://doi.org/10.1021/acs.analchem.8b03773.
- (10) Kuzman, D.; Bunc, M.; Ravnik, M.; Reiter, F.; Žagar, L.; Bončina, M. Long-Term Stability
   Predictions of Therapeutic Monoclonal Antibodies in Solution Using Arrhenius-Based
   Kinetics. *Sci Rep* 2021, *11*, 20534. https://doi.org/10.1038/s41598-021-99875-9.
- 498 (11) Majdinasab, M.; Badea, M.; Marty, J. L. Aptamer-Based Lateral Flow Assays: Current
   499 Trends in Clinical Diagnostic Rapid Tests. *Pharmaceuticals (Basel)* 2022, *15* (1), 90.
   500 https://doi.org/10.3390/ph15010090.
- (12) Maher, S.; Kamel, M.; Demerdash, Z.; El Baz, H.; Sayyouh, O.; Saad, A.; Ali, N.; Salah,
   F.; Atta, S. Gold Conjugated Nanobodies in a Signal-Enhanced Lateral Flow Test Strip for
   Rapid Detection of SARS-CoV-2 S1 Antigen in Saliva Samples. *Sci Rep* 2023, *13*, 10643.
   https://doi.org/10.1038/s41598-023-37347-y.
- Yang, L. F.; Kacherovsky, N.; Panpradist, N.; Wan, R.; Liang, J.; Zhang, B.; Salipante, S.
   J.; Lutz, B. R.; Pun, S. H. Aptamer Sandwich Lateral Flow Assay (AptaFlow) for
   Antibody-Free SARS-CoV-2 Detection. *Anal. Chem.* 2022, 94 (20), 7278–7285.
   https://doi.org/10.1021/acs.analchem.2c00554.
- (14) Stoltenburg, R.; Reinemann, C.; Strehlitz, B. SELEX—A (r)Evolutionary Method to
   Generate High-Affinity Nucleic Acid Ligands. *Biomolecular Engineering* 2007, 24 (4),
   381–403. https://doi.org/10.1016/j.bioeng.2007.06.001.
- (15) Ledsgaard, L.; Kilstrup, M.; Karatt-Vellatt, A.; McCafferty, J.; Laustsen, A. H. Basics of
   Antibody Phage Display Technology. *Toxins (Basel)* 2018, 10 (6), 236.
   https://doi.org/10.3390/toxins10060236.
- (16) Chevalier, A.; Silva, D.-A.; Rocklin, G. J.; Hicks, D. R.; Vergara, R.; Murapa, P.; Bernard,
  S. M.; Zhang, L.; Lam, K.-H.; Yao, G.; Bahl, C. D.; Miyashita, S.-I.; Goreshnik, I.; Fuller,
  J. T.; Koday, M. T.; Jenkins, C. M.; Colvin, T.; Carter, L.; Bohn, A.; Bryan, C. M.;
  Fernández-Velasco, D. A.; Stewart, L.; Dong, M.; Huang, X.; Jin, R.; Wilson, I. A.; Fuller,
  D. H. Balan, D. Maningla, Banallal de Nara, Particip Paring for Target at Theorematics
- D. H.; Baker, D. Massively Parallel de Novo Protein Design for Targeted Therapeutics.
- 520 *Nature* **2017**, *550* (7674), 74–79. https://doi.org/10.1038/nature23912.
- 521 (17) Watson, J. L.; Juergens, D.; Bennett, N. R.; Trippe, B. L.; Yim, J.; Eisenach, H. E.; Ahern,
  522 W.; Borst, A. J.; Ragotte, R. J.; Milles, L. F.; Wicky, B. I. M.; Hanikel, N.; Pellock, S. J.;

- Courbet, A.; Sheffler, W.; Wang, J.; Venkatesh, P.; Sappington, I.; Torres, S. V.; Lauko,
  A.; De Bortoli, V.; Mathieu, E.; Ovchinnikov, S.; Barzilay, R.; Jaakkola, T. S.; DiMaio, F.;
  Baek, M.; Baker, D. De Novo Design of Protein Structure and Function with RFdiffusion.
  Nature 2023, 620 (7976), 1089–1100. https://doi.org/10.1038/s41586-023-06415-8.
- (18) Cao, L.; Goreshnik, I.; Coventry, B.; Case, J. B.; Miller, L.; Kozodoy, L.; Chen, R. E.;
  Carter, L.; Walls, A. C.; Park, Y.-J.; Strauch, E.-M.; Stewart, L.; Diamond, M. S.; Veesler,
  D.; Baker, D. De Novo Design of Picomolar SARS-CoV-2 Miniprotein Inhibitors. *Science*2020, 370 (6515), 426–431. https://doi.org/10.1126/science.abd9909.
- (19) Gupta, R.; Gupta, P.; Wang, S.; Melnykov, A.; Jiang, Q.; Seth, A.; Wang, Z.; Morrissey, J. J.; George, I.; Gandra, S.; Sinha, P.; Storch, G. A.; Parikh, B. A.; Genin, G. M.;
  Singamaneni, S. Ultrasensitive Lateral-Flow Assays via Plasmonically Active Antibody-Conjugated Fluorescent Nanoparticles. *Nat. Biomed. Eng* 2023, 1–15.
  https://doi.org/10.1038/s41551-022-01001-1.
- (20) Xu, R.; Shi, M.; Li, J.; Song, P.; Li, N. Construction of SARS-CoV-2 Virus-Like Particles
   by Mammalian Expression System. *Frontiers in Bioengineering and Biotechnology* 2020,
   8.
- (21) Wilson, B. D.; Eisenstein, M.; Soh, H. T. Comparing Assays via the Resolution of
   Molecular Concentration. *Nat. Biomed. Eng* **2022**, *6* (3), 227–231.
   https://doi.org/10.1038/s41551-021-00832-8.
- 542 (22) Kunert, R.; Reinhart, D. Advances in Recombinant Antibody Manufacturing. *Appl Microbiol Biotechnol* **2016**, *100* (8), 3451–3461. https://doi.org/10.1007/s00253-016-7388-9.
- (23) Amasawa, E.; Kuroda, H.; Okamura, K.; Badr, S.; Sugiyama, H. Cost–Benefit Analysis of
   Monoclonal Antibody Cultivation Scenarios in Terms of Life Cycle Environmental Impact
   and Operating Cost. ACS Sustainable Chem. Eng. 2021, 9 (42), 14012–14021.
   https://doi.org/10.1021/acssuschemeng.1c01435.
- (24) Jyothilekshmi, I.; Jayaprakash, N. S. Trends in Monoclonal Antibody Production Using
   Various Bioreactor Systems. *J Microbiol Biotechnol* 2021, 31 (3), 349–357.
   https://doi.org/10.4014/jmb.1911.11066.
- (25) Cardoso, V. M.; Campani, G.; Santos, M. P.; Silva, G. G.; Pires, M. C.; Gonçalves, V. M.;
  de C. Giordano, R.; Sargo, C. R.; Horta, A. C. L.; Zangirolami, T. C. Cost Analysis Based
  on Bioreactor Cultivation Conditions: Production of a Soluble Recombinant Protein Using
  Escherichia Coli BL21(DE3). *Biotechnol Rep (Amst)* 2020, 26, e00441.
  https://doi.org/10.1016/j.btre.2020.e00441.
- (26) Schmideder, A.; Weuster-Botz, D. High-Performance Recombinant Protein Production with
   Escherichia Coli in Continuously Operated Cascades of Stirred-Tank Reactors. *Journal of Industrial Microbiology and Biotechnology* 2017, 44 (7), 1021–1029.
   https://doi.org/10.1007/s10295-017-1927-y.
- (27) Pepeliaev, S.; Ehebauer, M. T. Cultivation of Microbial Cultures at High Cell Density in
   Microbioreactor Fermentations to Increase Protein Yield. *Biotechnology and Applied Biochemistry* 2023, 70 (3), 1121–1127. https://doi.org/10.1002/bab.2425.
- (28) Choi, H.; Jung, Y. Applying Multivalent Biomolecular Interactions for Biosensors.
   *Chemistry A European Journal* 2018, 24 (72), 19103–19109.
   https://doi.org/10.1002/chem.201801408.
- (29) Errington, W. J.; Bruncsics, B.; Sarkar, C. A. Mechanisms of Noncanonical Binding
   Dynamics in Multivalent Protein–Protein Interactions. *Proceedings of the National*

569 Academy of Sciences **2019**, 116 (51), 25659–25667. 570 https://doi.org/10.1073/pnas.1902909116.

596

597

598

599

- (30) Errico, J. M.; Zhao, H.; Chen, R. E.; Liu, Z.; Case, J. B.; Ma, M.; Schmitz, A. J.; Rau, M. J.;
  Fitzpatrick, J. A. J.; Shi, P.-Y.; Diamond, M. S.; Whelan, S. P. J.; Ellebedy, A. H.; Fremont,
  D. H. Structural Mechanism of SARS-CoV-2 Neutralization by Two Murine Antibodies
  Targeting the RBD. *Cell Reports* 2021, 37 (4), 109881.
  https://doi.org/10.1016/j.celrep.2021.109881.
- 576 (31) Gosselin, B.; Retout, M.; Jabin, I.; Bruylants, G. Development of a Peptide-Based Lateral 577 Flow Assay for the Detection of the Cancer Biomarker Mdm2. *Sensors & Diagnostics* 578 **2024**, *3* (2), 248–255. https://doi.org/10.1039/D3SD00253E.
- (32) Lee, A. S.; Kim, S. M.; Kim, K. R.; Park, C.; Lee, D.-G.; Heo, H. R.; Cha, H. J.; Kim, C. S.
   A Colorimetric Lateral Flow Immunoassay Based on Oriented Antibody Immobilization for
   Sensitive Detection of SARS-CoV-2. Sensors and Actuators B: Chemical 2023, 379,
   133245. https://doi.org/10.1016/j.snb.2022.133245.
- 583 (33) Kim, H.; Choi, H.; Heo, Y.; Kim, C.; Kim, M.; Kim, K. T. Biosensors Based on Bivalent 584 and Multivalent Recognition by Nucleic Acid Scaffolds. *Applied Sciences* **2022**, *12* (3), 585 1717. https://doi.org/10.3390/app12031717.
- (34) Hao, L.; Li, X.; Liang, H.; Lei, W.; Yang, W.; Zhang, B. Biosensors Based on Potent
   Miniprotein Binder for Sensitive Testing of SARS-CoV-2 Variants of Concern. *Microchim Acta* 2023, 191 (1), 38. https://doi.org/10.1007/s00604-023-06113-2.
- 589 (35) Jelić, D. Thermal Stability of Amorphous Solid Dispersions. *Molecules* **2021**, *26* (1), 238. 590 https://doi.org/10.3390/molecules26010238.
- (36) Puthussery, J. V.; Ghumra, D. P.; McBrearty, K. R.; Doherty, B. M.; Sumlin, B. J.;
  Sarabandi, A.; Mandal, A. G.; Shetty, N. J.; Gardiner, W. D.; Magrecki, J. P.; Brody, D. L.;
  Esparza, T. J.; Bricker, T. L.; Boon, A. C. M.; Yuede, C. M.; Cirrito, J. R.; Chakrabarty, R.
  K. Real-Time Environmental Surveillance of SARS-CoV-2 Aerosols. *Nat Commun* 2023,
  14 (1), 3692. https://doi.org/10.1038/s41467-023-39419-z.
  - (37) Lin, C.; Liu, Z.; Fang, F.; Zhao, S.; Li, Y.; Xu, M.; Peng, Y.; Chen, H.; Yuan, F.; Zhang, W.; Zhang, X.; Teng, Z.; Xiao, R.; Yang, Y. Next-Generation Rapid and Ultrasensitive Lateral Flow Immunoassay for Detection of SARS-CoV-2 Variants. *ACS Sens.* **2023**, *8* (10), 3733–3743. https://doi.org/10.1021/acssensors.3c01019.
- (38) Lednicky, J. A.; Lauzardo, M.; Fan, Z. H.; Jutla, A.; Tilly, T. B.; Gangwar, M.; Usmani,
  M.; Shankar, S. N.; Mohamed, K.; Eiguren-Fernandez, A.; Stephenson, C. J.; Alam, M. M.;
  Elbadry, M. A.; Loeb, J. C.; Subramaniam, K.; Waltzek, T. B.; Cherabuddi, K.; Morris, J.
  G.; Wu, C.-Y. Viable SARS-CoV-2 in the Air of a Hospital Room with COVID-19
  Patients. *International Journal of Infectious Diseases* 2020, 100, 476–482.
  https://doi.org/10.1016/j.ijid.2020.09.025.
- (39) Ang, A. X.; Luhung, I.; Ahidjo, B. A.; Drautz-Moses, D. I.; Tambyah, P. A.; Mok, C. K.;
  Lau, K. J.; Tham, S. M.; Chu, J. J. H.; Allen, D. M.; Schuster, S. C. Airborne SARS-CoV-2
  Surveillance in Hospital Environment Using High-Flowrate Air Samplers and Its
  Comparison to Surface Sampling. *Indoor Air* 2022, 32 (1), e12930.
  https://doi.org/10.1111/ina.12930.